Uncertainties in tidally adjusted estimates of sea level rise flooding (bathtub model) for the Greater London

remote sensing

MDPI

Article

Uncertainties in Tidally Adjusted Estimates of Sea Level Rise Flooding (Bathtub Model) for the Greater London

Ali P. Yunus [1,*], Ram Avtar [1,2], Steven Kraines [3], Masumi Yamamuro [1], Fredrik Lindberg [4] and C. S. B. Grimmond [5]

1 Graduate School of Frontier Sciences, The University of Tokyo, Kashiwanoha 277-8563, Japan; avtar@unu.edu (R.A.); yamamuro@k.u-tokyo.ac.jp (M.Y.)
2 Institute for the Advanced Study of Sustainability (UNU-IAS), United Nations University, Tokyo 150-8925, Japan
3 Faculty of Liberal Arts and Sciences, Tokyo City University, Tokyo 158-8557, Japan; steven@kraines.net
4 Department of Earth Sciences, University of Gothenburg, Göteborg SE-405 30, Sweden; fredrikl@gvc.gu.se
5 Department of Meteorology, University of Reading, Reading RG6 6BB, UK; c.s.grimmond@reading.ac.uk
* Correspondence: yunusp@csis.u-tokyo.ac.jp; Tel.: +91-955-737-7666

Academic Editors: Yudong Tian, Ken Harrison, Magaly Koch and Prasad S. Thenkabail
Received: 7 December 2015; Accepted: 20 April 2016; Published: 28 April 2016

Abstract: Sea-level rise (SLR) from global warming may have severe consequences for coastal cities, particularly when combined with predicted increases in the strength of tidal surges. Predicting the regional impact of SLR flooding is strongly dependent on the modelling approach and accuracy of topographic data. Here, the areas under risk of sea water flooding for London boroughs were quantified based on the projected SLR scenarios reported in Intergovernmental Panel on Climate Change (IPCC) fifth assessment report (AR5) and UK climatic projections 2009 (UKCP09) using a tidally-adjusted bathtub modelling approach. Medium- to very high-resolution digital elevation models (DEMs) are used to evaluate inundation extents as well as uncertainties. Depending on the SLR scenario and DEMs used, it is estimated that 3%–8% of the area of Greater London could be inundated by 2100. The boroughs with the largest areas at risk of flooding are Newham, Southwark, and Greenwich. The differences in inundation areas estimated from a digital terrain model and a digital surface model are much greater than the root mean square error differences observed between the two data types, which may be attributed to processing levels. Flood models from SRTM data underestimate the inundation extent, so their results may not be reliable for constructing flood risk maps. This analysis provides a broad-scale estimate of the potential consequences of SLR and uncertainties in the DEM-based bathtub type flood inundation modelling for London boroughs.

Keywords: sea-level rise; flooding; digital elevation model; risk; uncertainties

1. Introduction

Floods from sea surge will have significant impacts on the world's coastal zones, particularly considering the projected sea-level rise (SLR) [1]. The reported annual losses from flood hazards have reached tens of billions of US dollars (USD) in the past decade, and many hundreds of people are killed each year [2]. Recent reports from United Nation Environment Program (UNEP) indicate that one third of the coastal regions run a high risk of degradation, especially from infrastructure development and pollution. Given this magnitude of potential loss that a sea water flood could cause to human life, property, and the economy, flood inundation modelling in urbanized coastal regions is increasingly relevant. Planning and conservation practitioners require reliable scientific data to

conduct vulnerability assessments that identify which parts of their city could be inundated by a potential flood.

Several approaches have been applied on regional and global scales to map the coastal flood levels to SLR [3,4]. Many flood models use fluid dynamics to simulate different hydrodynamic conditions. However, complexities in the urban environment and lack of proper hydrologic data often compromise the effectiveness of those models [5]. Static modelling techniques provide an alternative with less data requirements to assess the maximum inundation extent for a given combination of SLR and sea surge.

The estimate of areas that are expected to experience SLR inundation depends not only on the complexity or simplicity of the flood modelling approach, but also on the elevation data used. Gesch [6] showed that the accuracy of the elevation data determines the predicted vulnerability of urban coasts to the effects of flooding events. This accuracy, however, varies considerably depending on the source. Historically, topographic maps and photogrammetric methods were employed as the source of elevation data. Because heights are obtained from contour lines, the elevation data are intrinsically limited by the gap between contours of the topographic maps [7].

Since 2000, digital elevation models (DEMs) derived from satellite data are increasingly used for flood mapping [8]. Today, DEMs are generated from different sources and techniques such as photogrammetric methods using stereo pair aerial photographs and satellite data [9], terrestrial and airborne laser scanning [10,11], radar interferometry [12], and structure from motion techniques [13,14]. Increased sophistication of satellite remote sensing techniques has made it possible to construct global DEMs that provide elevation data for all of the land masses of the world. However, global DEMs typically have significantly lower accuracy and resolution than DEMs constructed using more proximate sensing techniques, such as airborne Light Detection And Ranging (LiDAR).

From the acquisition stage of the raw base data to the development of a DEM, a large number of measurements are involved [15]. Each of these are subject to some level of error and uncertainty. Errors introduced during data collection [16] arise due to excessive smoothing [17], transformation [18], and positioning [19]. The errors and uncertainties can occur in both the vertical (Z) and horizontal (XY) coordinates. Cooper [20] categorized errors in DEMs into: (a) gross errors (result of user error or equipment failure), (b) systematic errors (due to deterministic bias in the data collection or processing), and random errors (from the great variety of measurement operational tasks in producing the DEM). These errors and uncertainties can affect the reliability and usefulness of DEM-based flood analyses. Several researchers have investigated methods such as visual analysis and statistical approaches to identify the errors in the DEMs [21–24]. Diagnostic visualization of errors rely mostly on summary graphs and DEM-derived outputs such as slope and shaded reliefs [23]. The most common statistical descriptor to measure the errors in DEM is the root mean square error [23,25]. However, Fisher [23] suggested that the use of standard deviation and mean error provides a better description of the statistical distribution of the error.

The objectives of this research are to investigate how estimates of inundation extents are affected by the vertical uncertainty of different DEMs and to examine the effect of different inundation models on quantifying flood risk. The study area is one of the largest cities in Europe, London (Figure 1). London, home to greater than 8.5 million people, has an average population density of 5223 people/km^2. Currently, 1.5 million people and 300,000 properties are estimated to be located in the tidal flood risk area [26]. The 33 boroughs of Greater London cover an area of 1573 km^2 (Figure 1).The city is expected to continue to grow in population and to expand further into the adjoining Thames estuary. The city is the economic hub of the UK but also plays a central role in international commerce. Much of the commercial areas are located close to the tidal River Thames, notably the City of London and Canary Wharf (within Tower Hamlets).

London experiences a high risk of flooding along the stretches of the River Thames, with more than 350 km^2 (22.25%) located in the floodplain zone [27]. A large part of central London was developed on low-lying land alongside River Thames by large-scale reclamation of marshes and mudflats in the 17th century [28]. London's Strategic Flood Frame Work (LSFFW) team identifies three major

types of flooding in the London risk register: surface flooding during intense rain, inundation of flood plains by river water, and tidal-surge flooding [29]. Surface flooding in the city occurs when rainfall exceeds natural or piped drainage capacity and excess water collects in low lying and flat areas. During heavy rainfall, rain water can fill the low lying areas quickly with little or no warning. Fluvial flooding results from a river overtopping its banks and can occur within 30 min of the onset of rain [26]. Tidal flooding in the Greater London (Figure 1) occurs during the high tide conditions or during storm events. The tidal area of the Thames stretches from Sheerness and Shoeburyness in the east to Teddington Weir in the west (Figure 1). Major influences on tidal flooding of London are the volume of water already in the river, the height of the astronomical tide (HAT) and the surge level.

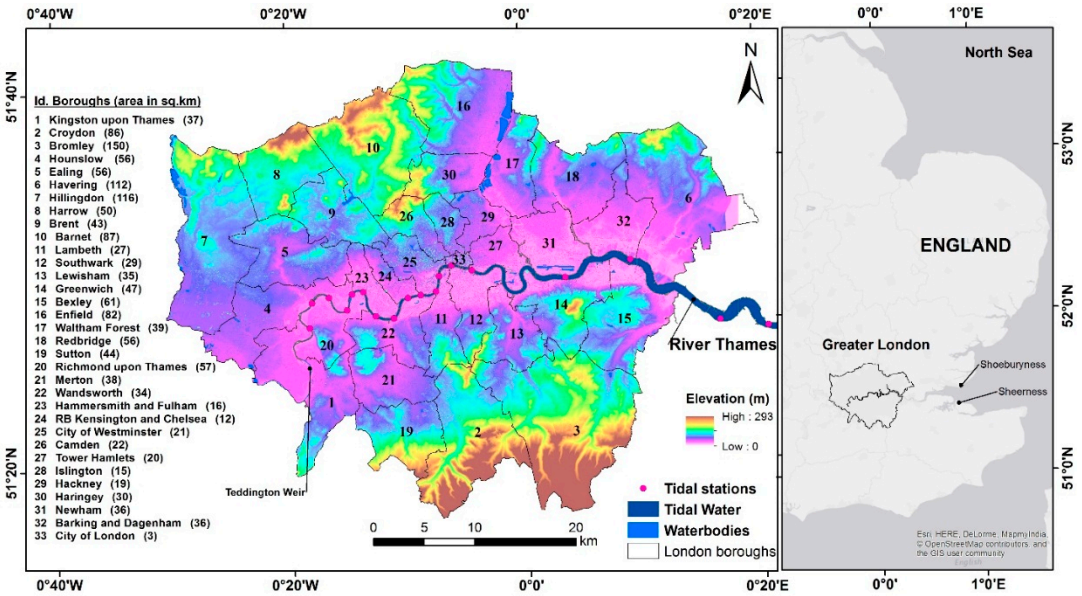

Figure 1. (**left**) the boroughs that constitute Greater London and Greater London's (**right**) location within southern England and. The topographical (LiDAR) elevation (m), the River Thames, Greater London boroughs with area (km^2), and locations mentioned in the text are labelled.

The historical record of flooding along the Thames Estuary dates back to the Anglo Saxon Chronicle of 1099 [28]. Localized flooding in London from the Thames is now perceived as a major risk [27,30]. The Houses of Parliament, Whitehall, City Hall, Canary Wharf, Westminster Abbey, the Tower of London, Kew Gardens, and the O2 Arena are all in flood risk areas. These areas also have several schools, hospitals, train stations, power stations, and substations, which would be damaged if sea water flooding was to occur [27]. The other flood-prone areas identified by the UK Environment Agency include large parts of the boroughs of Southwark, Lambeth, Tower Hamlets, Hammersmith, Fulham, Wandsworth, Barking, Dagenham, Woolwich and Newham together with many residential areas in Essex and Kent [27,30].

Marsh [31] identified that the major risk of flooding in London at present is from storm surges during low-pressure conditions and high winds that intensify tidal peaks. Tidal circulation in the Thames is driven by gravitational forcing, density variations due to salinity, and wind stress [32]. The average daily range of water levels in the Thames estuary is about 7 m [27]. However, during low pressure conditions, the water levels in the estuary can be increased by surge from the North Sea. As low pressure depressions move across the Atlantic towards the British Isles a bulge of water is created in its path. A surge tide happens when this mass of water moves down the east coast of England. The funnel shape of the Thames estuary leads the entering surge to increase water levels by 1 to 3 m, causing a major flood threat, especially if occurring during a "spring" tide (higher than normal tide levels) [27].

Global warming-enhanced sea levels will increase this risk by giving rise to dangerous tide levels. Additional risk is caused by the subsidence in the southeast of England of about 1.5 mm a year [30]. Several flood defenses are installed in the Thames estuary and its banks. The most prominent one is the Thames Barrier, which spans a width of 520 m across the river and protects 125 km^2 of central London from flooding. The Environment Agency reports that, as of April 2015, the Thames Barrier has been closed 175 times since it started operation in 1982. Of these closures, 88 were to protect against tidal flooding [27,30]. The frequency of the closure has increased tremendously in recent years, with 48 closures in 2014 [27].

2. Data and Methods

Using the data and methods described below, we conducted an elevation-based assessment of tidally-adjusted sea-level rise inundation vulnerability for the Greater London area for a "no protection scenario". This assumes the Thames without the current flood defenses, *i.e.*, the large embankments and Thames Barrier, because the DEMs used in this study do not incorporate detailed engineering-grade structures. Water levels in the Thames estuary are considered as they would appear during the mean highest high tide (MHHW).

2.1. Elevation Data Sources

DEMs come from a number of sources (topographic maps, photogrammetry, LIDAR, IFSAR) in a variety of forms with different datum and coordinate systems which are dependent on the source agency. However, almost all consist of records that contain gridded arrays of numbers which represent the ground elevation above sea level [23]. In the literature, the terms DEM (Digital Elevation Model), DTM (Digital Terrain Model), and DSM (Digital Surface Model) are all used to refer to these gridded arrays of numbers. A DEM is understood to be a raster or a set of vector contours, in which the pixel values represent the ground elevation above sea level over a specific area of the Earth. A DSM is a raster in which the pixel values represent the elevations above sea level of the ground and all features on it, including the tops of buildings, trees, and any other objects in addition to the natural terrain. A DEM can be edited to generate a DTM, which is a representation of a bare-Earth model that contains elevations of natural terrain features where vegetation, buildings, and other non-ground objects have been digitally removed [33]. Hence, the DSM elevation is higher in urban and forested areas than the DTM. Here, we use the term DEM as the general term for DSMs and DTMs, unless otherwise indicated. To resolve the datum conflicts between data sources, all the DEMs are projected into OSGB 1936 datum with OSTN02 rubber sheet transformation applied.

2.1.1. Ordnance Survey DEM

Two of the DEMs we analyze are from the Ordnance Survey (OS), UK. The first, the OS open data elevation model called OS Terrain 50, has a grid spacing of 50 m [34] and covers the entirety of Great Britain. It is available in tiles of 10 × 10 km. This DEM, developed originally using photogrammetric methods, is updated annually using other OS datasets. The required DEM tiles for Greater London were download from the Ordnance Survey [34] website. The second is a high-resolution DEM called OS Terrain 5 with a grid spacing of 5 m. With the greater accuracy "significant" landscape features can be included [35]. This dataset is regularly updated from the large scale OS database, which should ensure real-world representation. The OS Terrain 5 data are available in 5 km × 5 km tiles and were ordered through http://digimap.edina.ac.uk/ [35]. Both datasets are available as "bare earth" representation (buildings and vegetation excluded), so they can be considered to be DTMs. In the literature, the term DEM is often used as a generic form for both DTMs and DSMs. The OS Terrain 5 and OS Terrain 50 m DTMs used in this study are, hereafter, referred to as "5 m DEM" and "50 m DEM" respectively, unless otherwise indicated.

2.1.2. LiDAR DEM

A very high-resolution airborne LiDAR dataset procured in the summers of 2005 and 2008, which covers the entire Greater London [36], was also used in this study. The point clouds obtained from LiDAR source were processed at 1 m grid spacing. The DEM used in this study was not treated for the removal of surface features, such as buildings, and therefore is a DSM. This was resampled into 5, 10, 30, and 50 m grids in order to compare the results with the OS Terrain data and SRTM DEM. Bilinear interpolation techniques, which take a weighted average of the nearest cells, were used in the resampling because they are preferable to cubic and nearest neighbour techniques for DEM resampling [37–39]. The resampled LiDAR DEMs are hereafter referred as 5 m DEM_{Re}, 10 m DEM_{Re}, 30 m DEM_{Re} and 50 m DEM_{Re}.

2.1.3. SRTM DEM

The Shuttle Radar Topography Mission (SRTM) DEM, with a spatial resolution of approximately 30 m, was also used. This mission was flown aboard the space shuttle Endeavour in 2000 to create the first near-global digital elevation dataset. The NASA (National Aeronautics and Space Administration), NGA (National Geospatial-Intelligence Agency), ASI (Italian Space Agency) and DLR (German Aerospace Center) collaborated to create the SRTM DEM using interferometric radar. From the difference of two radar images taken at slightly different angles, the surface elevation is calculated [40]. SRTM data were obtained from EarthExplorer (http://earthexplorer.usgs.gov/) at a resolution of 1 arc-second (30 m) [41].

2.2. Inundation Model

The bathtub inundation model assumes that an area with an elevation less than a projected flood level will be flooded like a "bathtub". Flooding areas are determined through a simple calculation procedure in a GIS environment where the elevation in each cell of a DEM is compared against a predicted sea level and all cells with values lower than the predicted sea level are considered flooded. As only elevation data are required for its application, it permits estimates when detailed hydrological data is absent (which is often the case). The "bathtub" can be filled in two ways: with and without hydrological connectivity [42]. Bathtub models that consider hydrological connectivity, e.g., the passage of water from one cell to another, require that in addition to being below the flood level, an area must be hydrologically connected to the source of the flooding (e.g., the ocean or river) for it to be inundated. Several studies have applied bathtub models to map coastal flood inundation around the globe using both non-connected and hydrologically-connected methods [43,44]. Vaan de Sante *et al.* [42] and others suggested that a simulation with hydrological connectivity is more appropriate because a coastal flood directly influences only the adjacent land zone.

Following Poulter and Halpin [45], in this study two approaches are adopted to simulate flood inundation using SRTM and the other DEMs. The first approach, which does not consider hydrological connectivity, is a zero-way rule in which a raster cell is flooded if its elevation is less than the projected sea level. The second approach considers hydrological connectivity by simulating that a raster cell will be flooded if its elevation is below the projected sea level and if it is connected to a cell that is either flooded or open water. Here, the eight-way connectivity rule is used, so a raster cell is considered to be connected to all eight surrounding cells in both its cardinal and diagonal directions. Figure 2 describes the differences between different approaches. Although the bathtub model has several documented limitations [46,47], we believe that it is a satisfactory approach for our study, because we focus primarily on how estimates of inundation extents are affected by the vertical uncertainty of different DEMs.

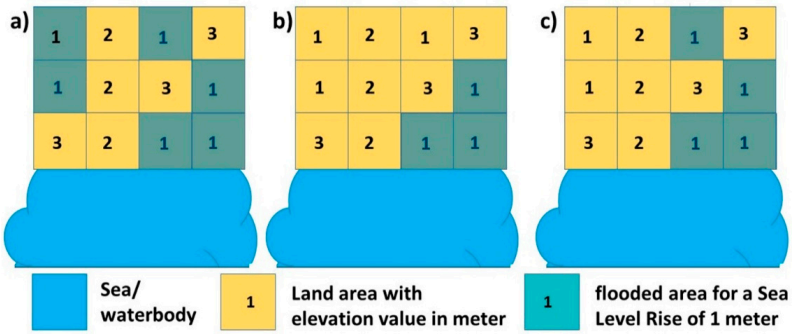

Figure 2. Different bathtub approaches: (**a**) zero-connectivity rule which shows that all the cells in the raster having elevation value ⩽1 m are flooded; (**b**) four-way hydrological connectivity rule for 1 m SLR where a cell is flooded only if it is connected to a water body directly or via adjacent cells in cardinal directions; and (**c**) eight-way hydrological connectivity rule for 1 m SLR where a cell is flooded only if it is connected to a water body directly or via adjacent cells in either cardinal or diagonal directions.

2.3. Projected Sea Level Rise

Three scenarios of SLR are considered based on the literature concerned with global (Section 2.3.1) and regional (Section 2.3.2) scales. These are: (i) 0.68 m by 2095 (UKCP09 for London); (ii) 0.82 m by 2100 (RCP8.5); and (iii) 1.9 m by 2100 (UKCP09 high++ for London).

2.3.1. Global

Global sea levels are projected to continue to rise beyond the 21st century as thermal expansion and melting of glaciers progress [48,49]. The IPCC Fourth Assessment Report [50] gives a global scenario estimated range (5th to 95th percentile) of 0.18–0.59 m SLR between present day (assuming a 1980–1999 baseline) and 2100. However, it is likely that the rate of global mean SLR during the 21st century will exceed the rate observed during the baseline period due to increases in ocean warming, melting of glaciers, ice caps, and a combined contribution from the Greenland and Antarctic ice sheets [1]. Improved process based models which account for land-ice contributions show 5% to 95% ranges of global mean SLR projections to be 0.26 to 0.55 m for Representation Concentration Pathway (RCP) 2.6; 0.32 to 0.63 m for RCP4.5; 0.33 to 0.63 m for RCP6.0; and 0.45 to 0.82 m for RCP8.5 [1].

2.3.2. Regional

Although almost all world coastlines are experiencing a rise in sea level, natural modes of climate variability, tectonic movements, subsidence by compaction, and anthropogenic factors influence the magnitude of SLR in different regions and times [48]. Sea levels around the United Kingdom (UK) have risen by about 1 mm/ year over the last century [51]. Defra guidance [51] projected a 0.90 m SLR for London by 2100, based on the maximum global mean sea level range climate scenario. The UKCP09 estimates that SLR for London will be approximately 0.21–0.68 m by 2095 [52]. The UKCP09 also modelled a worst case scenario that gives SLRs of up to 1.9 m by 2100 (high++ scenario); however, it is noted that this is highly unlikely. These estimates take into account the land movement in the region. In addition, the UKCP09 projection models account for ocean carbon cycle feedbacks, uncertainty due to natural variability, and other uncertainties associated with the modelling and statistical processing which were not included in the previous projections [51].

2.4. Tidal Surface Creation

To incorporate the tidal variability within the Thames estuary, a "modelled" surface that represents the same vertical datum as the elevation data is needed. The Port of London Authority (PLA) hydrographic service manages tidal information and predictions from several tide gauges along the River Thames and estuary. The mean highest high tide (MHHW) information for 23 sites along the river and estuary were obtained from the PLA handbook of tide tables 2009 (http://www.pla.co.uk/) (Figure 1). For incorporating tidal variability in the study region, we followed the simplest approach

given in the NOAA's Sea Level Rise tool [53]. First, we created a point shapefile for the tide gauge stations in ArcGIS using their latitude, longitude, together with MHHW information and the datum conversion factor. We then interpolated a raster surface by inverse distance weighted from the point tide gauges. Finally, we added the SLR for each of the scenarios to this surface (Section 2.3). In order to obtain inundation extents of the total land area from the river and sea only, the inland water bodies were screened out in the flooding area estimation. Additionally, removing the inland waterbodies should reduce errors in the estimates, although the data may be incomplete for areas, such as small canals and ditches.

2.5. Accuracy Assessment

To investigate the accuracy of DEMs and uncertainty in the projected inundation levels, the absolute vertical accuracies of all six DEMs (1 m DEM, 5 m DEM_{Re}, 5 m DEM, 30 m DEM_{Re}, 30 m SRTM DEM, and 50 m DEM) were estimated in ArcGIS relative to independent reference points from Ordnance Survey, UK. The reference points (3539 spot heights on ground distributed across the east of England) include 38 within Greater London that were used to measure the accuracy of DEMs.

Root mean square error (RMSE), which has become a standard measure of the map accuracies of elevation datasets [6,54], is calculated in this study:

$$RMSE = \sqrt{\frac{\sum \left(Z_{dem} - Z_{ref}\right)^2}{n}} \quad (1)$$

where Z_{dem} is the vertical coordinate of the check points in the elevation dataset, Z_{ref} is the high-accuracy spot height in the reference dataset, and n is the number of points checked. The National Standard for Spatial Data Accuracy (NSSDA) measurement of linear error (LE_{95}) with a 95% confidence level is calculated from:

$$LE_{95} = 1.96 * RMSE$$

Mean error is calculated using the following equation:

$$ME = \frac{\sum Z_{dem} - Z_{ref}}{n}$$

ME can be either negative or positive; a negative value of the ME tells us that the measurements consistently underestimate the true values, while a positive ME indicates the opposite [23].

3. Results

For several reasons, the future sea level rise is uncertain (Section 2.3). Of the three scenarios (UKCP09 London (0.68 m), RCP8.5 of IPCC (0.82 m) and UKCP09 high ++ London (1.9 m)) simulated for the end of the century, we consider the UKCP09 high++ London scenario as the most likely because recent studies [55,56] argue that the sea-level rise is likely to exceed 1 m by 2100.

3.1. Scenario 1: 0.68 m SLR UKCP09

Using the eight-way connectivity bathtub approach with a projected SLR of 0.68 m from the present MHHW, about 17 boroughs of Greater London (GL) with a total surface area of between 0.01 km^2 and 14.9 km^2 are predicted to be inundated (Figure 3a and Table A1). The largest absolute areas of inundation are predicted for Newham (11.55–14.29 km^2), Southwark (4.10–12.91 km^2), Greenwich (6.13–8.89 km^2), Havering (6.57–8.77 km^2), and Barking and Dagenham (6.04–8.07 km^2). The inundation for the total GL area is largest from the 5 m DEM (82.23 km^2) and smallest from SRTM DEM (49.87 km^2). The flooded areas predicted from 1 m DEM, 5 m DEM_{Re}, 30 m DEM_{Re}, and 50 m DEM are 61.76 km^2, 64.49 km^2, 61.64 km^2, and 63.51 km^2, respectively. In summary, the flood estimates of the eight-way connectivity are related as: 5 m DEM > 5 m DEM_{Re} > 50 m DEM > 1 m DEM > 30 m DEM_{Re} > SRTM DEM.

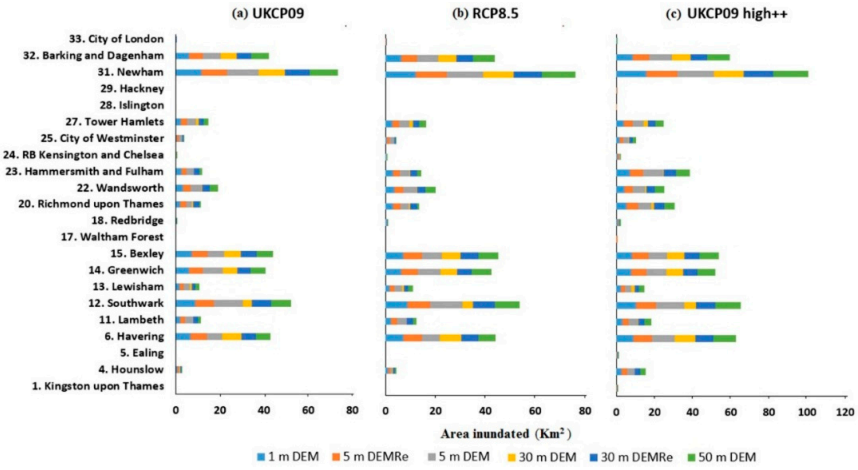

Figure 3. Inundation areas estimated for Greater London boroughs (km^2) obtained from an eight-way connectivity method using six different DEMs and three SLR scenarios: (**a**) 0.68 m UKCP09; (**b**) 0.82 m RCP 8.5; and (**c**) 1.9 m UKCP09 High++.

Using the same SLR (0.68 m), but with a non-connectivity approach, flood waters are predicted to reach all the mapped locations, and parts of 22 boroughs will be inundated (Figure 4a and Table A1), which is five more than the estimate from the eight-way connectivity approach. Again, the total flood areas estimated by the SRTM DEM (56.36 km^2) are much smaller than those estimated by the other DEM's. Estimated total inundation areas from 1 m DEM, 5 m DEM$_{Re}$, 5 m DEM, 30 m DEM$_{Re}$, and 50 m DEM are 68.24 km^2, 69.37 km^2, 87.95 km^2, 66.41 km^2, and 70.60 km^2, respectively. The total estimates of inundation areas from zero-connectivity approaches have a different ordering to the eight-way connectivity: 5 m DEM > 50 m DEM > 5 m DEM$_{Re}$ > 1 m DEM > 30 m DEM$_{Re}$ > SRTM DEM. However, the difference between the 5 m DEM$_{Re}$ and 50 m DEM estimates is small. Under this scenario, large parts of Greenwich, Havering, Bexley, Newham, Southwark, and Barking and Dagenham are predicted to be flooded to a depth of 2 m or more. The depths and spatial extents of flood inundation for the GL area obtained from different DEMs (except for 30 m DEM$_{Re}$) for scenario 1 are shown in Figure 5a–e. The difference between inundation extents from 5 m DEM$_{Re}$ and 30 m DEM$_{Re}$ was found to be insignificant. The boroughs having the largest estimated percentage impact are Southwark (14.17%–44.76%) and Newham (31.90%–40.27%) followed by Hammersmith and Fulham (0.58%–28.11%), Barking and Dagenham (16.75%–24.17%) and Tower Hamlets (6.21%–20.32%).

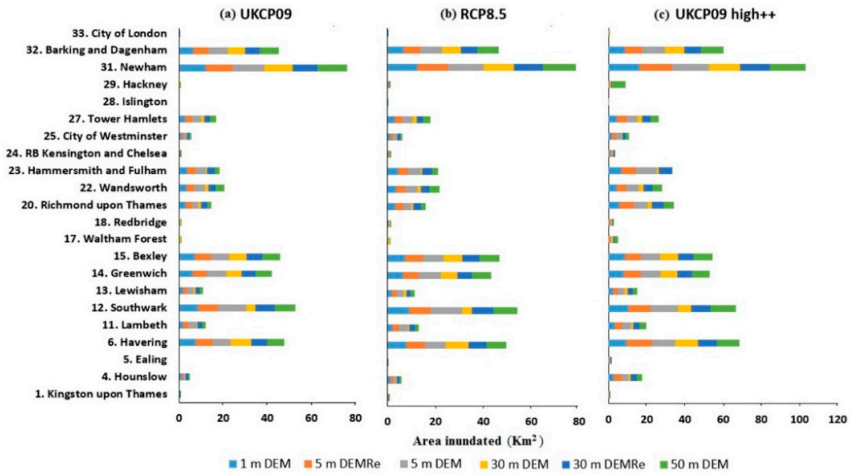

Figure 4. Inundation areas estimated for Greater London boroughs (km^2) obtained from a zero-connectivity method using six different DEMs and three SLR scenarios: (**a**) 0.68 m UKCP09; (**b**) 0.82 m RCP 8.5; and (**c**) 1.9 m UKCP09 High++.

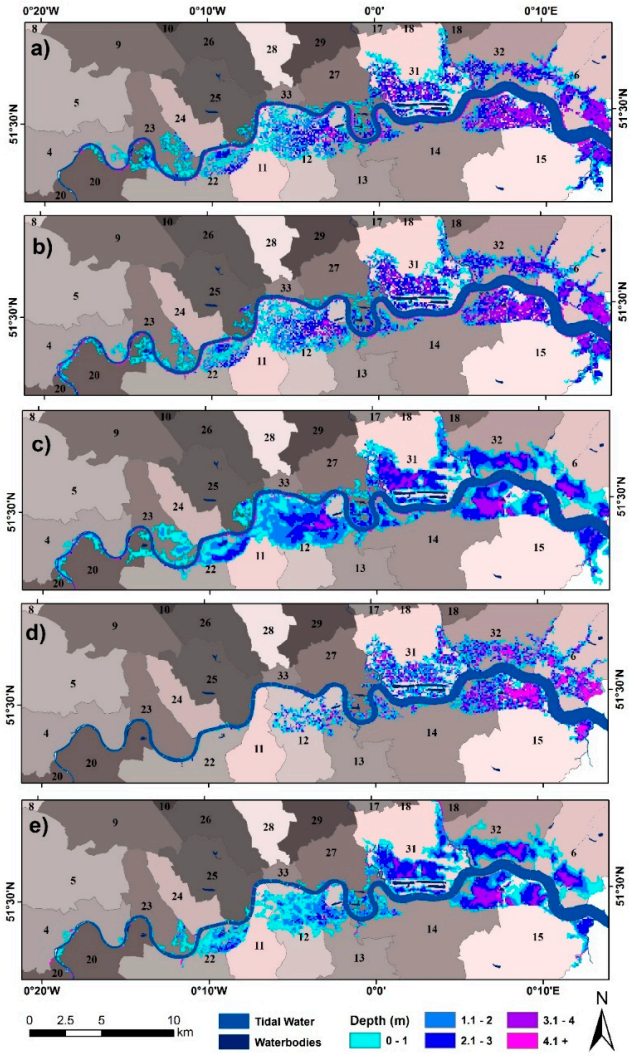

Figure 5. Flood depths obtained for inundated Greater London boroughs from the eight-way hydrological connectivity approach by UKCP09 sea-level rise scenario of 0.68 m. (**a**) 1 m LiDAR DEM; (**b**) 5 m LiDAR DEM$_{Re}$; (**c**) 5 m DEM; (**d**) 30 m SRTM DEM; and (**e**) 50 m DEM. Figure 1 gives the borough names that correspond to the numbers.

3.2. Scenario 2: 0.82 m SLR RCP8.5

Under the 0.82 m SLR scenario, the eight-way connectivity approach predicts flooding extents of 49.87 to 87.26 km^2 or 3.16%–5.5% of the total GL area (1573 km^2) (Figure 3b and Table A2). The RCP8.5 estimates are approximately 0–5 km^2 larger than the UKCP09 0.62 m SLR (Section 3.1). The 0.14 m larger SLR is predicted to cause about a 5.8% increase in flooded areas with the 1 m DEM, 5.2% with the 5 m DEM$_{Re}$, 5.7% from the 5 m DEM, 4.4% from the 30 m DEM$_{Re}$, and 7% from the 50 m DEM. Because the SRTM DEM elevations are only given as integers, the increase of 0.14 m from UKCP09 does not make any difference in the flood level estimates. Borough level estimates for flooding areas by the eight-way connectivity bathtub model are similar to the UKCP09 estimates, with the RCP 8.5 also suggesting Newham (11.99–14.87 km^2) and Southwark (4.10–13.10 km^2) to be the most vulnerable areas followed by Greenwich (6.27–9.12 km^2) and Barking and Dagenham (6.25–8.45 km^2) (Figure 3b and Table A2).

The difference between the areas estimated by the eight-way connectivity approach and the zero-connectivity approach for the RCP8.5 projection from different DEMs is 4.09–6.77 km^2 (Figures 3b and 4b, Table A2). The number of boroughs partly inundated from the RCP8.5 projection

again increases from 17 to 22 in the zero-connectivity approach. Unlike the UKCP09 scenario, the RCP8.5 projection has the same DEM ordering of the flood areal extent from both approaches: 5 m DEM > 50 m DEM > 5 m DEM$_{Re}$ > 1 m DEM > 30 m DEM$_{Re}$ > SRTM DEM. Figure 6 shows the flood depth for London boroughs in scenario 2. The depths and spatial extents of flood inundation for the GL area obtained from different DEMs are shown in Figure 6a–e. Although the largest flooding extent is estimated for Newham and Southwark, the flood depth is greatest in Bexley, Havering, and Greenwich boroughs (Figure 6a–e). Overall, flood depth decreases towards the Teddington Wier from Sheerness and Shoeburyness. The boroughs with the largest percentage impact are the same as for the UKCP09 scenario but with slightly larger values: Southwark (14.17%–45.45%), Newham (33.03%–41.73%), Hammersmith and Fulham (0.58%–33.78%), Barking and Dagenham (17.33%–25%), and Tower Hamlets (6.21%–21.43%).

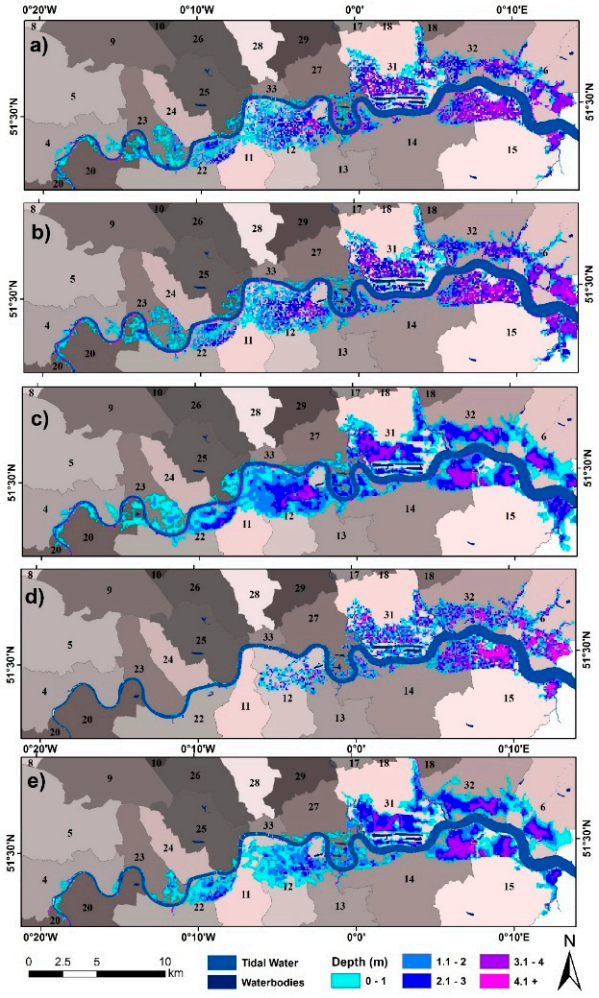

Figure 6. Flood depths obtained for inundated London boroughs from the eight-way hydrological connectivity approach by RCP8.5 global sea-level rise scenario of 0.82 m. (**a**) 1 m LiDAR DEM; (**b**) 5 m LiDAR DEM$_{Re}$; (**c**) 5 m DEM, (**d**) 30 m SRTM DEM; and (**e**) 50 m DEM. Figure 1 gives the borough names that correspond to the numbers.

3.3. Scenario 3: 1.90 m SLR UKCP09 High++

Using the eight-way connectivity approach, 67–125 km^2 of GL land area is predicted to be inundated from the 1.9 m SLR (UKCP09 high++); including about 15.36–19.30 km^2 in Newham (Figure 3c and Table A3). Among the other boroughs, Southwark (6.24–14.63 km^2), Barking and Dagenham (8.53–11.92 km^2), Havering (8.89–12.16 km^2), Bexley (8.2–10 km^2), and Hammersmith and Fulham (0.39–10.52 km^2) have large areal impacts (Figure 3c and Table A3). The UKCP09 high++

scenario results in flood levels that are 28.55% higher than RCP8.5 and 32.70% higher than UKCP09 with the 1 m DEM; 29.51% higher than RCP8.5 and 33.54% higher than UKCP09 with the 5 m DEM_{Re} estimate; 30.18% higher than RCP8.5 and 34.21% higher than UKCP09 for the 5 m DEM estimate; 25.27% higher than both RCP8.5 and UKCP09 for the SRTM DEM estimate; and 37.37% higher than RCP8.5 and 41.79% higher than UKCP09 for the 50 m DEM estimate. The spatial extent of flood inundations for the GL UKCP09 high++ projections are shown in Figure 7. The zero-connectivity model shows a total flood estimate of 77.78–127.14 km^2 of the GL area (Figure 4c and Table A3). The increased percentage of flood estimates for UKCP09 high++ varies between 21.42%–40.79% for RCP8.5 and 21.42%–45.62% for UKCP09 estimates. The spatial extent of flood inundation under UKCP09 high++ projections (Figure 7) show some flooding areas covered by >3 m. It is apparent (Figure 7e) that the flood depths in Lewisham and Southwark obtained from 50 m DEM are largely underestimated when compared to the results from other DEMs (Figure 7a–c).

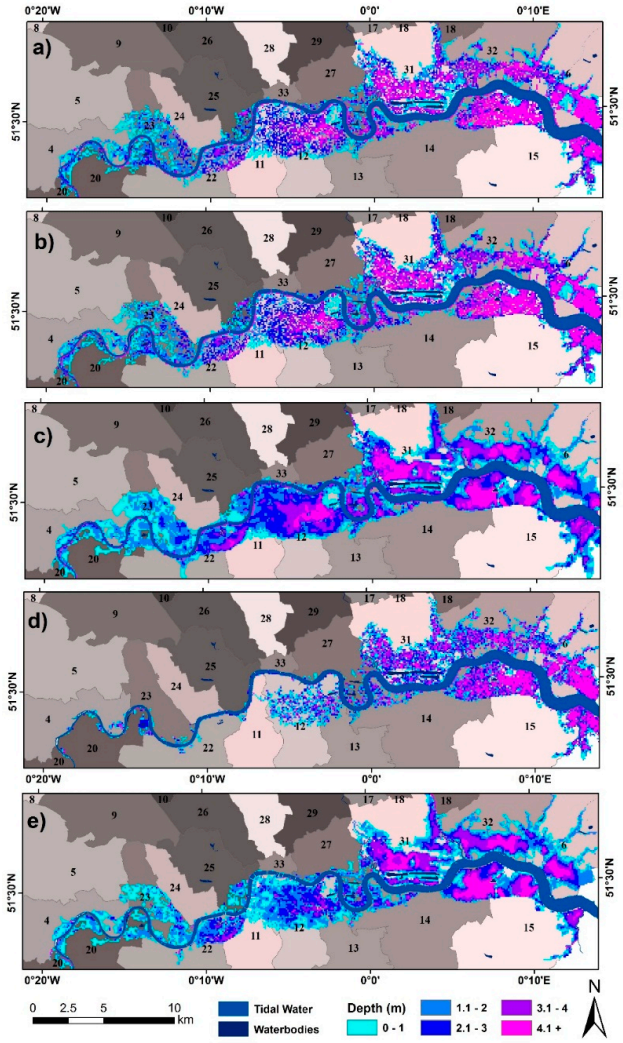

Figure 7. Flood depths obtained for inundated London boroughs from the eight-way hydrological connectivity approach by UKCP09 high++ sea-level rise scenario of 1.90 m. (**a**) 1 m LiDAR DEM; (**b**) 5 m LiDAR DEM_{Re}; (**c**) 5 m DEM; (**d**) 30 m SRTM DEM; and (**e**) 50 m DEM. Figure 1 gives the borough names that correspond to the numbers.

3.4. RMSE, NSSDA, and ME Estimation

The descriptive statistics for the six DEMs used (Table 1) suggest that, as expected, the 1 m, resampled 5 m and 30 m LiDAR DEMs have the best agreement with the "true" values obtained from the spot height data. The RMSE estimated for these three DEMs are between 0.61 and 0.67 m, which

is both considerably better than the other three DEMs and close to industry standards for LiDAR data [57]. The RMSEs estimated for the 5 m OS Terrain and 50 m OS Terrain data are 1.19 and 1.17 m, respectively. Although the RMSE for SRTM DEM (3.33 m) is the largest, like other studies [7,58], we found that it is still better than the product specification (9.73 m). Moreover the ME of SRTM is better than that of OS Terrain DEMs (Table 1). The corresponding NSSDA standards for vertical accuracies are also shown in Table 1. Assuming that the DEMs meet the NSSDA standards, the best accuracy that could be expected at a 95% confidence level is 1.21 m as given by the LiDAR DEM.

Table 1. Root mean square error (RMSE), national standard for spatial data accuracy (NSSDA) measurement of linear error (L.E.) with a 95% confidence level, and mean error (ME) for the different DEMs used in this study.

Elevation Data	Approx. Resolution (m)	RMSE (m)	NSSDA (m) (95%)	ME
LiDAR 1 m	1	0.67	1.33	−0.001
LiDAR 5 m DEM_{Re}	5	0.66	1.30	−0.05
5 m DEM OS data	5	1.19	2.35	−0.84
LiDAR 30 m DEM_{Re}	30	0.61	1.21	−0.02
SRTM 30 m DEM	30	3.33	6.54	−0.40
50 m DEM OS data	50	1.17	2.30	−0.79

4. Discussion

DEMs with very fine resolutions developed from interferometric SAR techniques and relatively straightforward sources, such as terrestrial and airborne LiDAR, are increasingly available, particularly for urban regions. These DEMs can provide accurate delineation of topographical vulnerabilities to natural phenomenon including flooding. For instance, Gesch [7] used a 3 m LiDAR DEM to map SLR flooding in parts of the United States; Cooper *et al.* [59] used 1.3 m LiDAR for flood mapping in Kahului Harbor, Hawaii; and Zhang [60] employed a 1.5 m LiDAR to derive inundation polygons in South Florida. In the past, when no high-resolution DEM was available, 30 second SRTM DEM, ASTER GDEM, 1 arc second SRTM DEM, and GTOPO 30 have been used in many parts of the world by various researchers for inundation studies [3,61]. In addition, regionally available national elevation data [44] and the recently developed TanDEM-X DEM [54] are also useful for flood inundation studies. As noted previously, DEMs derived from different sources and techniques often have varying resolutions and levels of uncertainty.

A previous study in the Thames estuary estimated an area of about 1000 km^2 to be inundated [33]; however, that study used an unlikely global scale SLR. Rowley *et al.* [3] also used unlikely hypothetical SLR values of up to 6 m for mapping inundation levels and did not account for the tidal variability in their analysis. Although our study does not use a hydrodynamic simulation, we apply a simpler bathtub flood model to very likely SLR scenarios for GL using high-resolution topographic data and accounting for the tidal variability in the Thames estuary. The results suggest that the high-resolution DEMs are effective for estimating flooding areas and pinpointing hotspots of potential vulnerability in GL. However, the inundation estimates vary greatly depending on the source and techniques used to construct the elevation model and on the hydrological connectivity assumptions.

The main goals of this analysis included understanding the impacts of the different DEMs in flood modelling, as well as the hydrological connectivity approaches. Strauss *et al.* [44] noted the impact of methodology chosen with respect to SLR threshold projection and hydrological connectivity to the water bodies. Several previous studies indicate that an eight-way connectivity model produces more reasonable results than a zero-connectivity approach [7,42]. These studies provide an improved understanding of the dynamic effect of flow models and contribute to an overall transition beyond the simple threshold-only "bathtub" approach.

Our results are in agreement with these previous studies. Figure 8 demonstrates the hydrological connectivity issue: the red areas (Figure 8a) indicate very low elevation topography. Although the violet and cyan pixels in Figure 8b, corresponding to the red colour in Figure 8a, have low elevation, only cyan coloured pixels are hydrologically connected to the tidal Thames and, therefore, have high

chances of flooding. By using such a hydrologically-connected approach, we find that the overall inundation extent estimates decrease between 1.68 km^2 and 12.01 km^2 when compared with the zero-connectivity method (Figures 3 and 4 Tables A1–3). Indeed, boroughs that are distant to the Thames (e.g., Hackney and Waltham Forest) are flooded with the zero connectivity approach. Although the inundation extent of these boroughs are smaller, considering their spatial location, inundation seems to be unrealistic and so the zero connectivity approach probably results in overestimation of the inundation extent. Therefore, we only discuss the inundation extents estimated by the eight-way connectivity model in the following.

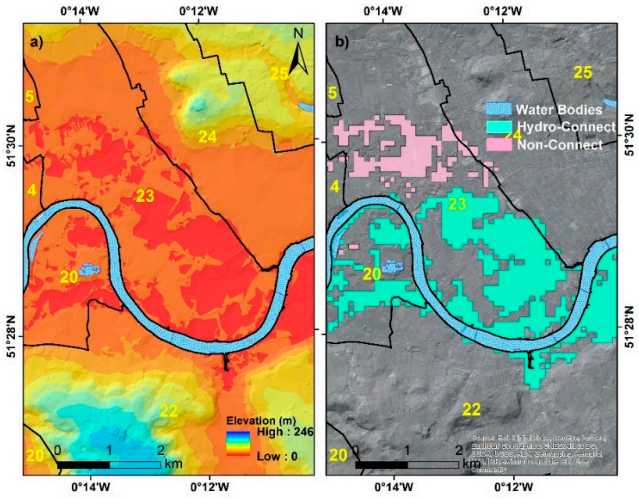

Figure 8. Example showing hydrologically-connected and non-connected pixels in Greater London for a sea-level rise (SLR) of 0.82 m. (**a**) Topography depicted from 5 m OS DEM; (**b**) cells under SLR flood risk and connected to the Thames estuary (cyan) and non-connected cells (violet). Higher elevation areas (e.g., part of borough 24) are not flooded from a SLR of 0.82 m.

Varying flood inundation polygons are obtained for GL for the same SLR scenarios with different DEMs (Section 3). For instance, under the UKCP09 scenario, the area of GL estimated to be flooded varies from 61 km^2 (1 m DEM and resampled 30 m DEM), to 64 km^2 (resampled 5 m DEM, and 50 m DEM), to 82 km^2 (5 m DEM from Ordnance Survey), to 49 km^2 (SRTM DEM) (Table A1). These differences in inundation extents estimated from different DEMs may be due to one or more of the following:

(i) artefacts in the DEM resulting from the measurement source,
(ii) artefacts introduced at the production stage,
(iii) differences in processing methodology, and
(iv) varying resolution of DEMs.

Indeed, even a small error in the DEM data can produce very different inundation polygons, particularly when using the hydrological connectivity approach (Tables A1–A3). The order of the RMSEs for the DEMs is: 30 DEM$_{Re}$ < 5 m DEM$_{Re}$ < 1 m DEM < 50 m DEM < 5 m DEM < SRTM DEM. Although 30 m and 5 m DEM$_{Re}$ are derived from 1 m DEM, they show higher accuracy. This is probably because of the smoothening effect of the bilinear interpolation technique [62]. This effect of resampling is demonstrated in Figure 9a. Resampling DEM from 1 to 5 m produces a difference of less than 1 m elevation for about 90% of total area in GL, 1–3 m for about 6% of total area and 3–5 m for about 3% of total area. This difference varies with resampling resolution (Figure 9a).

It is curious that the estimates of flood areas from the 5 m DEM are considerably higher than those of the 1 m DEM and its resampled products. These differences are likely attributable to the processing of the DEMs. As noted, the airborne LiDAR derived 1 m DEM and DEM$_{Re's}$ function as Digital Surface Models (DSMs), whereas the photogrammetrically-derived 5 m DEM and 50 m DEM from OS are

Digital Terrain Models (DTMs). A DTM is a 'bare earth' elevation model where vegetation and other surface features, such as buildings, have been identified and removed, whereas a DSM includes these surface objects.

The differences in 5 m and 50 m OS DEMs are shown in Figure 9b. Since 1 m DEM and 5 m DEM_{Re} data include surface objects, they tend to exclude the areas of buildings from the estimates of flooding areas. On the other hand, in a DTM areas having buildings that are below the flood level will be included in the flood area. Figure 9c shows that approximately 16% of the area in GL is underestimated in >3 m category for the DTM compared to the DSM, whereas overestimation is only 1% for the same category. This indicates that the DTM contains significantly lower elevation values, which results in a greater flooded area than a DSM. Griffin *et al.* [63] argued that the best approach for modelling flood inundation is to use a DTM together with an appropriate surface roughness condition, but their studies deal with tsunami inundation where the water flow has the force to destroy buildings. For SLR flooding, the ideal DEM may lie between a DSM and a DTM, because some structures may resist flow, while others allow water to flow through them and may even collapse with prolonged flooding. Furthermore, future SLR flooding predictions cannot be validated *a priori*, unlike riverine flood or tsunami inundation models. Hence, there is need to develop methods to assess what DEM is optimal for simulating tidally-adjusted SLR inundations.

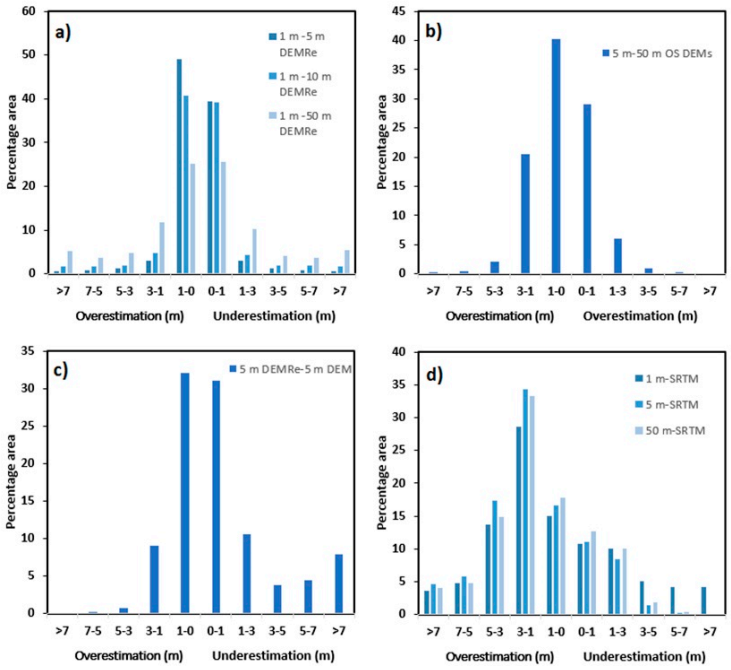

Figure 9. Percentage of areas overestimated and underestimated in DEMs when: (**a**) resampled 5 m DEM_{Re}, 10 m DEM_{Re}, and 50 m DEM_{Re}, are compared with the original 1 m LiDAR DEM, (**b**) 50 m OS DEM is compared to the 5 m OS DEM, (**c**) 5 m OS DEM (DSM) is compared to the resampled 5 m DEM_{Re}, and (**d**) SRTM elevations DEM is compared with the other elevation datasets.

Our results also show that SRTM DEM underestimates the flooded areas compared to the higher accuracy DEMs. Large areas west of the City of London (code 33) are estimated to be flooded according to the LiDAR DEMs and OS Terrain data, but they are not included in the flood inundation zones mapped by SRTM DEM (Figures 5 and 6). Estimated flood inundation areas obtained from SRTM DEM are about 11–25 km^2 smaller than the 1 m DEM predictions. Similar results are also found with the resampled 5 m and 30 m LiDAR DEM_{Re}. This large difference may be because: (i) SRTM DEM (3.33 m RMSE) has large inaccuracies in vertical accuracy compared to the other DEMs, and (ii) flooded polygons can only be determined for whole-metre increments because the vertical increment of the SRTM-DEM is 1 m. The latter results in identical estimates of flooded areas for the UKCP09 and RCP8.5 scenarios when using SRTM DEM (Section 3).

Elevations in the low-lying areas are often overestimated in SRTM DEM [54,64,65]. Figure 10 demonstrates the vertical inaccuracies in elevation values in SRTM DEM for GL. When compared SRTM elevation pixels with the 50 m DEM, it can be seen that most parts of boroughs 33 (City of London), 25 (Westminster), 24 (Kensington and Chelsea), and 26 (Camden) are in the category of overestimated pixels (Figure 10a). Comparison with 5 m DEM shows similar overestimates (Figure 10d). The red area (Fig 10a) has the most tall buildings in London. Thus, it appears that SRTM DEM is a surface model rather than a terrain model. The percentage of pixels overestimated by the SRTM DEM compared to other DEMs (Figure 9d) is much larger (about 66%–74% of total area) than that of the underestimated elevation pixels, which explains the large underestimation in flooding extent. The peaks in the underestimated elevation areas for the categories greater than 3 m in the comparison of the SRTM DEM with the 1 m DEM may be attributed to the higher accuracy of LiDAR DEM in estimating building heights (Figure 9d, Figure 10c).

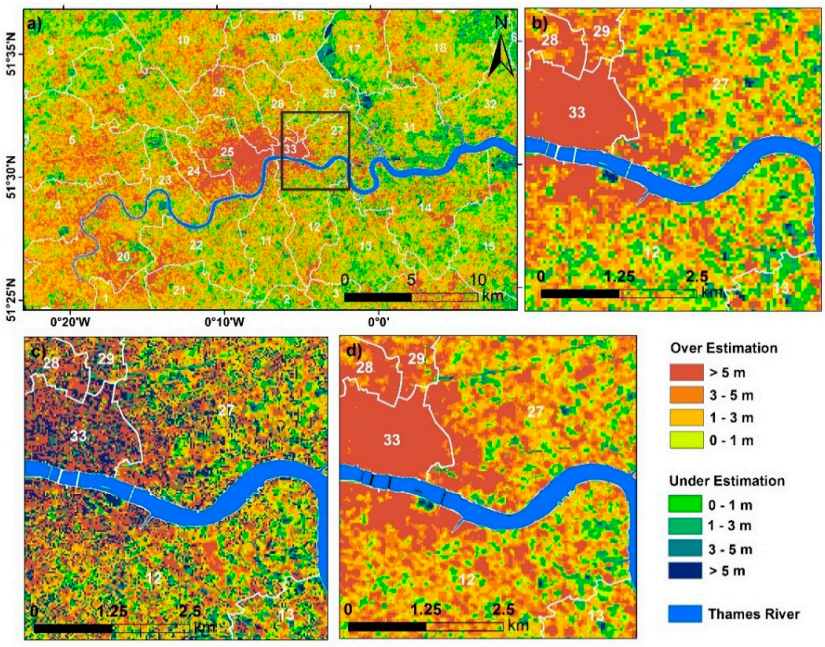

Figure 10. Location of overestimated and underestimated elevation pixels in SRTM DEM compared to (**a**) 50 m DEM with square box shown in detail in (**b**), (**c**) 1 m DEM, and (**d**) 5 m DEM.

The horizontal resolution of the DEM affects the delineation of inundation zones to resolve flow through and around individual features, which may help to explain the differences in inundation extents using SRTM DEM versus using of other DEMs (Figures 3 and 4 Tables A1–3). The difference in inundation extent between SRTM DEM and the other DEMs increases from lower to higher SLR projections. It appears that given the low accuracy of SRTM DEM, it may only be useful for identifying large floodplains [66]. In this regard, Gallegos *et al.* [67] suggested that a horizontal resolution of 5 m may be required for detailed evaluation of risk assessment, so SRTM DEM may not have sufficient resolution to simulate flood inundation with confidence. Similar observations have been made in other studies [3,7,63]. However, the 50 m DEM, which is an OS derivative from 10 m contours using photogrammetric techniques that are updated annually using other high-resolution terrain datasets, provides much better estimates of the total flooded areas despite the low horizontal resolution [34]. For disaster prevention and mitigation purposes, we agree with Wang *et al.* [65], that an overestimation of the flood hazard is more desirable than underestimation. Hence, we recommend using the freely available 50 m open DEM data for inundation studies in UK, if no high-resolution data are available. However, the SRTM DEM is currently the best freely available global elevation dataset that could be used to generate inundation polygons for understanding risks and vulnerabilities. As Schumann *et al.* [68] suggest, if SRTM data are carefully processed and uncertainties are properly accounted for, they can be useful for the evaluation of flood models.

5. Conclusions

Different digital elevation data have been tested for modelling the extent of SLR flood inundation for three different scenarios in the Greater London area. The adapted bathtub approach and results presented in this study are useful alternatives to hydro-dynamic models considering computational requirements and data availability. We summarize the main conclusions of this study in the following statements:

(i) An eight-way connectivity bathtub approach gives significantly smaller flood inundation extents than the zero connectivity approach, indicating that the zero-connectivity approach may overestimate flooded areas due to the hydrological connectivity issue.

(ii) Large variability in inundation estimates is observed for the same SLR scenario when using different elevation datasets, and this is attributed to differences in horizontal and vertical resolution, as well as processing methodologies.

(iii) Flood inundation models developed using 1 m airborne LiDAR DEM give inundation extents between 61.76 and 91.77 km^2 for three different SLR scenarios; 5 m DEM$_{Re}$ gives 64.24–96.60 km^2; 5 m DEM gives 82.23–124.99 km^2, 30 m DEM$_{Re}$ gives 61.64–91.04 km^2, SRTM DEM gives 49.87–66.74 km^2 and 50 m DEM gives 63.51–109.13 km^2. Thus, while 1 m DEM, 5 m DEM$_{Re}$, 30 m DEM$_{Re}$, and 50 m DEM give similar inundation extents, the extents estimated by 5 m DEM are much larger, while the extents estimated by SRTM DEM are much smaller.

(iv) Differences in inundation areas estimated between DSMs and DTMs for the same SLR scenarios are considerably larger than the RMSE differences between the datasets. As expected, using DTMs tends to result in higher inundation extents while using DSMs tends to result in lower inundation extents. Thus, we recommend to use a DTM and add objects using a DSM that may considerably influence the prediction such as large buildings, pillars of bridges, etc.

(v) Flood inundation estimates using SRTM DEM appear to significantly underestimate inundation extents, possibly as a result of high RMSE and low vertical and horizontal resolution. Therefore, careful consideration should be made when assessing inundation zones from flood models using SRTM DEM.

(vi) Although there are concerns about using DEMs having low spatial resolution, we recommend that the regionally available open data 50 m DEM be used for inundation studies of the UK rather than SRTM DEM, if no high-resolution data are available.

Although this study illustrates the uncertainties regarding the modelling approach and elevation data, it does not account for flood protection measures or local hydrodynamics, including differences in roughness conditions for different types of land cover. Nevertheless, it demonstrates that even small differences in vertical accuracies of DEM have a strong effect on the quantitative assessment of the SLR inundation associated with climate change. In addition, the uncertainties related to both hydrological connectivity and processing levels must be assessed given the complexity of flood modelling.

Acknowledgments: Authors are grateful to NASA, USGS and Ordnance Survey, UK for providing the free DEMs to the scientific community. The authors would like to express sincere thanks to Japan Society of Promotion of Science, and Belmont Forum (NERC TRUC) for their kind support.

Author Contributions: Y.A., R.A., S.K., and M.Y. conceived and designed the study. Y.A. performed analyses of the data, drafted an initial version of the manuscript, and worked with co-authors on its improvements. C.S.B.G. and F.L. provided necessary data, facilities and significantly contributed to discussions, data analyzes and manuscript preparation. M.Y. is the Principle Investigator for Grant of the study.

Conflicts of Interest: The authors declare no conflict of interest.

Appendix

Table A1. Potential inundation areas for Greater London boroughs (in km^2) obtained from the 0.68 m UKCP09 London sea-level rise scenario as estimated from six different elevation datasets (Section 2.1) and two different connectivity (eight-way hydrological and zero) approaches (Section 2.2). Only the boroughs that will be impacted are included (compare with Figure 1). Bold values indicate boroughs having ⩾3 km^2 inundation areas.

Boroughs	**1 m DEM**		**5 m DEM$_{Re}$**		**5 m DEM**		**30 m DEM**		**30 m DEM$_{Re}$**		**50 m DEM**	
	8-way	*0-connect*	*8-way*	*0-connect*	*8-way*	*0-connect*	*8-way*	*0-connect*	*8-way*	*0-connect*	*8-way*	*0-connect*
1. Kingston upon Thames	-	0.14	-	0.14	-	-	-	0.03	-	0.17	-	0.03
4. Hounslow	0.59	1.08	0.69	1.01	0.45	0.91	0.17	0.24	0.72	1.10	0.38	0.78
5. Ealing	-	0.02	-	0.02	-	-	-	-	-	-	-	-
6. Havering	**6.78**	**7.61**	**7.34**	**7.59**	**6.83**	**8.17**	**8.77**	**9.37**	**6.70**	**7.29**	**6.57**	**7.8**
11. Lambeth	1.94	1.96	2.21	2.24	**3.74**	**3.79**	0.03	0.44	2.14	2.16	1.29	1.42
12. Southwark	**8.76**	**8.82**	**8.67**	**8.88**	**12.91**	**12.92**	**4.1**	**4.09**	**8.62**	**8.70**	**9.09**	**9.34**
13. Lewisham	1.66	1.71	1.83	1.87	2.82	2.83	0.96	1.18	1.64	1.65	1.7	1.72
14. Greenwich	**6.13**	**6.36**	**6.3**	**6.4**	**8.89**	**8.91**	**6.66**	**6.84**	**5.82**	**6.03**	**7.04**	**7.66**
15. Bexley	**7.19**	**7.28**	**7.34**	**7.43**	**7.38**	**8.06**	**7.56**	**7.96**	**7.06**	**7.18**	**7.64**	**7.9**
17. Waltham Forest		0.1		0.1		0.13		0.5		0.13		0.05
18. Redbridge	0.08	0.2	0.10	0.12	0.08	0.3	0	0.18	0.12	0.15	0.35	0.35
20. Richmond upon Thames	1.91	**3.00**	2.89	**3.00**	2.65	2.85	0.6	0.98	2.64	2.87	0.59	1.82
22. Wandsworth	**3.32**	**3.36**	**3.32**	**3.40**	**5.13**	**5.16**	0.28	1.44	**3.27**	**3.32**	**3.85**	**3.99**
23. Hammersmith and Fulham	2.64	**3.74**	2.1	**3.79**	**3.41**	**4.61**	0.09	0.5	2.39	**3.56**	1.34	2.11
24. RB Kensington and Chelsea	0.14	0.27	0.12	0.21	0.11	0.2	0.02	0.06	0.16	0.26	0.03	0.06
25. City of Westminster	0.54	1.06	0.85	1.05	1.47	1.5	0.06	0.1	0.62	1.05	0.18	0.8
27. Tower Hamlets	2.44	2.83	2.71	2.98	**3.94**	**4.02**	1.23	1.7	2.33	2.56	2.28	2.79
28. Islington		0.01		0.01		0.01			-			0.01
29. Hackney	-	0.08	-	0.14	-	0.2	-	0.19	-	0.08		0.08
31. Newham	**11.55**	**12.00**	**11.76**	**12.23**	**14.29**	**14.58**	**11.99**	**12.58**	**11.00**	**11.54**	**12.88**	**13.28**
32. Barking and Dagenham	**6.05**	**6.54**	**6.23**	**6.73**	**8.07**	**8.73**	**7.34**	**7.97**	**6.40**	**6.60**	**8.29**	**8.6**
33. City of London	0.05	0.05	0.02	0.02	0.06	0.06			0.01	0.01		
Total	61.76	68.24	64.49	69.37	82.23	87.95	49.87	56.36	61.64	66.41	63.51	70.6

Table A2. Potential inundation areas for Greater London boroughs obtained from the 0.82 m RCP8.5 global sea-level rise scenario as estimated from six different elevation datasets (Section 2.1) and two different connectivity (eight-way hydrological and zero) approaches (Section 2.2). Only the boroughs that will be impacted are included (compare with Figure 1). Bold values indicate boroughs having $\geqslant$3 km^2 inundation areas.

Boroughs	1 m DEM		5 m DEM$_{Re}$		5 m DEM		30 m DEM		30 m DEM$_{Re}$		50 m DEM	
	8-way	*0-connect*	*8-way*	*0-connect*	*8-way*	*0-connect*	*8-way*	*0-connect*	*8-way*	*0-connect*	*8-way*	*0-connect*
1. Kingston upon Thames		0.15		0.14		0.01		0.03		0.17		0.03
4. Hounslow	1.05	1.25	0.87	1.12	0.89	1.17	0.17	0.24	0.94	1.28	0.5	0.91
5. Ealing		0.04		0.04						0.04		
6. Havering	**7**	**7.9**	**7.45**	**7.72**	**7.23**	**8.68**	**8.77**	**9.37**	**6.90**	**7.56**	**6.9**	**8.26**
11. Lambeth	2.16	2.16	2.35	2.38	**3.95**	**3.96**	0.03	0.44	2.37	2.38	1.53	1.67
12. Southwark	**8.91**	**8.96**	**8.96**	**9.05**	**13.11**	**13.12**	**4.1**	**4.09**	**8.78**	**8.87**	**9.98**	**10.23**
13. Lewisham	1.7	1.75	1.94	1.98	2.87	2.87	0.96	1.18	1.71	1.73	1.86	1.87
14. Greenwich	**6.28**	**6.52**	**6.52**	**6.57**	**9.13**	**9.15**	**6.66**	**6.84**	**6.01**	**6.24**	**7.8**	**7.88**
15. Bexley	**7.26**	**7.37**	**7.4**	**7.49**	**7.95**	**8.41**	**7.56**	**7.96**	**7.13**	**7.26**	**7.94**	**8.13**
17. Waltham Forest		0.1		0.1		0.14		0.5		0.14		0.05
18. Redbridge	0.08	0.22	0.12	0.15	0.31	0.31		0.18	0.14	0.18	0.36	0.36
20. Richmond upon Thames	2.96	**3.27**	**3.17**	**3.29**	**3.07**	**3.26**	0.6	0.98	2.88	**3.06**	0.71	2.1
22. Wandsworth	**3.5**	**3.56**	**3.5**	**3.58**	**5.39**	**5.39**	0.28	1.44	**3.39**	**3.47**	**3.97**	**4.13**
23. Hammersmith and Fulham	2.94	**4.28**	2.84	**4.2**	**3.95**	**5.54**	0.09	0.5	2.78	**4.10**	1.62	2.52
24. RB Kensington and Chelsea	0.15	0.32	0.14	0.23	0.13	0.23	0.02	0.06	0.17	0.31	0.03	0.08
25. City of Westminster	0.62	1.16	1.06	1.17	1.72	1.72	0.06	0.1	0.66	1.10	0.21	0.95
27. Tower Hamlets	2.69	3	2.84	**3.13**	**4.18**	**4.24**	1.23	1.7	2.51	2.74	2.9	**3.02**
28. Islington		0.02		0.01		0.01						0.01
29. Hackney		0.12		0.16		0.23		0.19		0.09		0.08
31. Newham	**11.96**	**12.42**	**12.43**	**12.68**	**14.87**	**15.11**	**11.99**	**12.58**	**11.49**	**11.97**	**13.33**	**13.86**
32. Barking and Dagenham	**6.26**	**6.77**	**6.48**	**6.96**	**8.45**	**9.03**	**7.34**	**7.97**	**6.55**	**6.80**	**8.69**	**8.98**
33. City of London	0.06	0.06	0.03	0.03	0.06	0.06			0.02	0.02		
Total	65.57	71.42	68.09	72.18	87.26	92.64	49.87	56.36	64.43	69.51	68.34	75.11

Table A3. Potential inundation areas for Greater London boroughs obtained from the 1.90 meter UKCP09 high++ London sea-level rise scenario as estimated from six different elevation datasets (Section 2.1) and two different connectivity (eight-way hydrological and zero) approaches (Section 2.2). Only the boroughs that will be impacted are included (compare with Figure 1). Bold values indicate boroughs having ⩾3 km^2 inundation areas.

Boroughs	1 m DEM		5 m DEM$_{Re}$		5 m DEM		30 m DEM		30 m DEM$_{Re}$		50 m DEM	
	8-way	*0-connect*	*8-way*	*0-connect*	*8-way*	*0-connect*	*8-way*	*0-connect*	*8-way*	*0-connect*	*8-way*	*0-connect*
1. Kingston upon Thames			0.18	0.22		0.05		0.06	0.60	0.20	0.01	0.08
4. Hounslow	2.8	2.73	2.91	**3.91**	**3.82**	**3.85**	0.06	0.93	2.95	3.24	2.89	2.96
5. Ealing	0.22	0.24	0.24	0.38	0.31	0.31	0	0.01	0.27	0.27	0.01	0.03
6. Havering	**8.89**	**9.48**	**9.7**	**13.15**	**12.16**	**12.21**	**10.76**	**12.03**	**9.49**	**9.74**	**11.79**	**12.08**
11. Lambeth	**3.07**	**3.22**	**3.22**	**3.76**	**4.92**	**4.92**	0.3	0.9	**3.18**	**3.24**	**3.67**	**3.72**
12. Southwark	**10.37**	**10.51**	**10.51**	**11.34**	**14.63**	**14.64**	**6.24**	**6.65**	**10.31**	**10.32**	**13.39**	**13.39**
13. Lewisham	2.27	2.36	2.48	2.58	**3.28**	**3.36**	1.69	1.85	2.24	2.32	2.74	2.78
14. Greenwich	**7.84**	**8**	**8.05**	**8.72**	**10.54**	**10.61**	**8.5**	**8.55**	**7.65**	**7.75**	**9.5**	**9.57**
15. Bexley	**8.2**	**8.47**	**8.51**	**8.59**	**10**	**10.1**	**9.11**	**9.18**	**7.98**	**8.18**	**9.78**	**9.94**
17. Waltham Forest			0.5	0.69		0.66		1.14		0.52		2.04
18. Redbridge	0.47	0.4	0.43	0.5	0.56	0.56	0.02	0.37	0.38	0.39	0.54	0.54
20. Richmond upon Thames	**5.48**	**5.66**	**5.88**	**7.69**	**6.92**	**7.09**	1.42	2.31	**5.56**	**5.95**	**5.38**	**5.51**
22. Wandsworth	**4.24**	**4.31**	**4.49**	**5.02**	**6.46**	**6.46**	0.68	2.57	**4.33**	**4.51**	**5.09**	**5.15**
23. Hammersmith and Fulham	**7.14**	**6.78**	**6.92**	**7.57**	**10.52**	**10.69**	0.39	1.36	**6.29**	**6.68**	**7.23**	0.11
24. RB Kensington and Chelsea	0.63	0.5	0.67	0.92	0.78	0.82	0.03	0.1		0.71	0.33	0.34
25. City of Westminster	1.73	1.84	1.89	2.06	2.94	2.94	0.07	0.16	1.79	1.83	2.01	2.04
27. Tower Hamlets	**4.05**	**4.39**	**4.49**	**4.76**	**5.81**	**5.93**	2.17	2.71	**4.00**	**4.13**	**4.42**	**4.52**
28. Islington			0.01			0.01						0.01
29. Hackney			0.37	0.4	0.08	0.58		0.31		0.28		**7.23**
31. Newham	**15.76**	**16.02**	**16.31**	**17.22**	**19.3**	**19.37**	**15.36**	**16.22**	**15.51**	**15.78**	**18.39**	**18.63**
32. Barking and Dagenham	**8.53**	**8.51**	**8.81**	**9.07**	**11.81**	**11.83**	**9.93**	**10.38**	**8.45**	**8.70**	**11.92**	**11.92**
33. City of London	0.09	0.04	0.05	0.06	0.17	0.17			0.06	0.06	0.05	0.05
Total	91.77	93.45	96.6	108.61	124.99	127.14	66.74	77.78	91.04	94.76	109.13	112.65

References

1. Church, J.A.; Clark, P.U.; Cazenave, A.; Gregory, J.M.; Jevrejeva, S.; Levermann, A.; Merrifield, M.A.; Milne, G.A.; Nerem, R.S.; Nunn, P.D.; *et al.* Sea level change. In *Climate Change 2013: The Physical Science Basis. Contribution of Working Group I to the Fifth Assessment Report of the Intergovernmental Panel on Climate Change*; PM Cambridge University Press: Cambridge, UK; New York, NY, USA, 2013; pp. 1137–1216.
2. Hirabayashi, Y.; Mahendran, R.; Koirala, S.; Konoshima, L.; Yamazaki, D.; Watanabe, S.; Kim, H.; Kanae, S. Global flood risk under climate change. *Nat. Climate Chang.* **2013**, *3*, 816–821. [CrossRef]
3. Rowley, R.J.; Kostelnick, J.C.; Braaten, D.; Li, X.; Meisel, J. Risk of rising sea level to population and land area. *Eos, Trans. Am. Geophys. Union* **2007**, *88*, 105–116. [CrossRef]
4. Mcleod, E.; Poulter, B.; Hinkel, J.; Reyes, E.; Salm, R. Sea-Level rise impact models and environmental conservation: A review of models and their applications. *Ocean Coast. Manag.* **2010**, *53*, 507–517. [CrossRef]
5. Chen, J.; Hill, A.A.; Urbano, L.D. A GIS-based model for urban flood inundation. *J. Hydrol.* **2009**, *373*, 184–192. [CrossRef]
6. Gesch, D.B. Consideration of vertical uncertainty in elevation-based sea-level rise assessments: Mobile Bay, Alabama case study. *J. Coast. Res.* **2013**, *63*, 197–210. [CrossRef]
7. Gesch, D.B. Analysis of LiDAR elevation data for improved identification and delineation of lands vulnerable to sea-level rise. *J. Coast. Res.* **2009**, *10053*, 49–58. [CrossRef]
8. Li, J.; Wong, D.W. Effects of DEM sources on hydrologic applications. *Comput. Environ. Urban Syst.* **2010**, *34*, 251–261.
9. Tsanis, I.; Seiradakis, K.; Daliakopoulos, I.; Grillakis, M.; Koutroulis, A. Assessment of GeoEye-1 stereo-pair-generated DEM in flood mapping of an ungauged basin. *J. Hydroinf.* **2014**, *16*, 1–18. [CrossRef]
10. Langridge, R.; Ries, W.; Farrier, T.; Barth, N.; Khajavi, N.; De Pascale, G. Developing Sub 5-m LiDAR DEMs for forested sections of the alpine and hope faults, South Island, New Zealand: Implications for structural interpretations. *J. Struct. Geol.* **2014**, *64*, 53–66. [CrossRef]
11. Hayakawa, Y.S.; Oguchi, T.; Saito, H.; Kobayashi, A.; Baker, V.R.; Pelletier, J.D.; McGuire, L.A.; Komatsu, G.; Goto, K. Geomorphic imprints of repeated tsunami waves in a coastal valley in northeastern Japan. *Geomorphology* **2015**, *242*, 3–10. [CrossRef]
12. Jiang, H.; Zhang, L.; Wang, Y.; Liao, M. Fusion of high-resolution DEMs derived from COSMO-SkyMed and TerraSAR-X InSAR datasets. *J. Geodesy* **2014**, *88*, 587–599. [CrossRef]
13. Mancini, F.; Dubbini, M.; Gattelli, M.; Stecchi, F.; Fabbri, S.; Gabbianelli, G. Using unmanned aerial vehicles (UAV) for high-resolution reconstruction of topography: The Structure from motion approach on coastal environments. *Remote Sens.* **2013**, *5*, 6880–6898. [CrossRef]
14. Gomez, C.; Hayakawa, Y.; Obanawa, H. A Study of Japanese landscapes using structure from motion derived DSMs and DEMs based on historical aerial photographs: New opportunities for vegetation monitoring and diachronic geomorphology. *Geomorphology* **2015**, *242*, 11–20. [CrossRef]
15. Mukherjee, S.; Joshi, P.K.; Mukherjee, S.; Ghosh, A.; Garg, R.D.; Mukhopadhyay, A. Evaluation of vertical accuracy of open source digital elevation model (DEM). *Int. J. Appl. Earth Obs. Geoinform.* **2012**, *21*, 205–217. [CrossRef]
16. Rodriguez, E.; Morris, C.S.; Belz, J.E. A Global assessment of the SRTM performance. *Photogramm. Eng. Remote Sens.* **2006**, *72*, 249–260. [CrossRef]
17. Polidori, L.; Chorowicz, J.; Guillande, R. Description of terrain as a fractal surface, and application to digital elevation model quality assessment. *Photogramm. Eng. Remote Sens.* **1991**, *57*, 1329–1332.
18. Carter, J.R. The effect of data precision on the calculation of slope and aspect using gridded DEMs. *Cartographica* **1992**, *29*, 22–34. [CrossRef]
19. Triglav-Čekada, M.; Crosilla, F.; Kosmatin-Fras, M. A simplified analytical model for a-priori LiDAR point-positioning error estimation and a review of LiDAR error sources. *Photogramm. Eng. Remote Sens.* **2009**, *75*, 1425–1439. [CrossRef]
20. Cooper, M.A.R. Datums, coordinates and differences. In *Landform Monitoring, Modelling and Analysis*; Wiley: Chichester, UK, 1998; pp. 21–36.
21. Hunter, G.J.; Goodchild, M.F. Mapping uncertainty in spatial databases, putting theory into practice. *J. Urban Reg. Inf. Syst. Assoc.* **1993**, *5*, 55–62.

22. Kraus, K. Visualization of the quality of surfaces and their derivatives. *Photogramm. Eng. Remote Sens.* **1994**, *60*, 457–462.
23. Fisher, P.F.; Tate, N.J. Causes and consequences of error in digital elevation models. *Prog. Phys. Geogr.* **2006**, *30*, 467–489. [CrossRef]
24. Leon, J.X.; Heuvelink, G.B.M.; Phinn, S.R. Incorporating DEM uncertainty in coastal inundation mapping. *PLoS ONE* **2014**, *9*, e108727. [CrossRef] [PubMed]
25. Shearer, J.W. The accuracy of digital terrain models. In *Terrain Modelling in Surveying and Civil Engineering*; Petrie, G., Kennie, T.J.M., Eds.; Caithness, Whittles Publishing: New York, NY, USA, 1990; pp. 315–336.
26. Greater London Authority. Flooding. Available online: https://www.london.gov.uk/mayor-assembly/mayor/london-resilience/risks/flooding (accessed on 16 September 2015).
27. Environmental Agency. *TE2100 Plan. Managing Flood Risk Through London and the Thames Estuary*; Environmental Agency: London, UK, 2012.
28. Lavery, S.; Donovan, B. Flood risk management in the Thames estuary looking ahead 100 years. *Philos. Trans. Ser. A* **2005**, *363*, 1455–1474. [CrossRef] [PubMed]
29. Greater London Authority. London Resilience, London Strategic Flood Framework Version 2. Available online: https://www.london.gov.uk/sites/default/files/London-Strategic-Flood-Framework-V2_1.pdf (accessed on 12 April 2012).
30. Guardian. Beyond the Thames Barrier: How Safe is London from Another Major Flood? Available online: http://www.theguardian.com/cities/2015/feb/19/thames-barrier-how-safe-london-major-flood-at-risk (accessed on 13 August 2015).
31. Marsh, T.J. The Risk of Tidal Flooding in London. Climate, Hydrology, Sea Level and Air Pollution. Available online: http://www.ecn.ac.uk/iccuk/indicators/10.htm (accessed on 13 August 2015).
32. Dawson, R.J.; Hall, J.W.; Bates, P.D.; Nicholls, R.J. Quantified analysis of the probability of flooding in the Thames estuary under imaginable worst case sea-level rise scenarios. *Int. J. Water Res. Dev.* **2005**. [CrossRef]
33. Aeromatrex. Digital Elevation, Digital Terrain or Digital Surface Model? Available online: http://www.aeromatrex.co,.au/blog/?p=89 (accessed on 20 February 2016).
34. OS Terrain 50 DTM. Available online: http://www.Ordnancesurvey.Co.uk/opendata/ (accessed on 13 February 2015).
35. OS Terrain 5 DTM. [ASC Geospatial Data], Scale 1:10,000, Updated: 23 September 2014, Ordnance Survey (GB), Using: EDINA Digimap Ordnance Survey Service. Available online: http://digimap.edina.ac.uk (accessed on 2 February 2015).
36. Lindberg, F.; Grimmond, C.S.B.; Martilli, A. Sunlit fractions on urban facets—Impact of spatial resolution and approach. *Urban Clim.* **2015**, *12*, 65–84. [CrossRef]
37. Shi, W.; Wang, B.; Tian, Y. Accuracy analysis of digital elevation model relating to spatial resolution and terrain slope by bilinear interpolation. *Math. Geosci.* **2014**, *46*, 445–481. [CrossRef]
38. Lin, S.; Jing, C.; Coles, N.A.; Chaplot, V.; Moore, N.J.; Wu, J. Evaluating DEM source and resolution uncertainties in the soil and water assessment tool. *Stoch. Environ. Res. Risk Assess.* **2013**, *27*, 209–221. [CrossRef]
39. Zhou, Y.; Chen, J.; Guo, Q.; Cao, R.; Zhu, X. Restoration of information obscured by mountainous shadows through Landsat TM/ETM images without the use of DEM data: A new method. *IEEE Trans. Geosci. Remote Sens.* **2014**, *52*, 313–328. [CrossRef]
40. USGS. Shuttle Radar Topography Mission (SRTM) 1 Arc-Second Global. Available online: https://lta.Cr.Usgs.gov/SRTM1Arc (accessed on 16 September 2015).
41. JPL/NASA. U.S. Releases Enhanced Shuttle Land Elevation Data. Available online: http://www2.Jpl.Nasa.gov/srtm/ (accessed on 16 September 2015).
42. Vaan de Sante, B.; Lansen, J.; Claartje, H. Sensitivity of coastal flood risk assessments to digital elevation models. *Water* **2012**, *4*, 568–579. [CrossRef]
43. Titus, J.G.; Richman, C. Maps of lands vulnerable to sea level rise: Modeled elevations along the US Atlantic and Gulf Coasts. *Clim. Res.* **2001**, *18*, 205–228. [CrossRef]
44. Strauss, B.H.; Ziemlinski, R.; Weiss, J.L.; Overpeck, J.T. Tidally adjusted estimates of topographic vulnerability to sea level rise and flooding for the contiguous United States. *Environ. Res. Lett.* **2012**, *7*, 014033. [CrossRef]
45. Poulter, B.; Halpin, P.N. Raster modelling of coastal flooding from sea-level rise. *Int. J. Geogr. Inf. Sci.* **2008**, *22*, 167–182. [CrossRef]

46. Gallien, T.W.; Sanders, B.F.; Flick, R.E. Urban coastal flood prediction: integrating wave overtopping, flood defences and drainage. *Coast. Eng.* **2014**, *91*, 18–28. [CrossRef]
47. Seenath, A.; Wilson, M.; Miller, K. Hydrodynamic *versus* GIS modelling for coastal flood vulnerability assessment: Which is better for guiding coastal management. *Ocean Coast. Manag.* **2016**, *120*, 99–109. [CrossRef]
48. Wong, P.P.; Losada, I.J.; Gattuso, J.P.; Hinkel, J.; Khattabi, A.; McInnes, K.L.; Saito, Y.; Sallenger, A. *Coastal Systems and Low-Lying Areas. in: Climate Change 2014: Impacts, Adaptation, and Vulnerability. Part A: Global and Sectoral Aspects. Contribution of Working Group II to the Fifth Assessment Report of the Intergovernmental Panel on Climate Change*; Field, C.B., Barros, V.R., Dokken, D.J., Mach, K.J., Mastrandrea, M.D., Bilir, T.E., Chatterjee, M., Ebi, K.L., Estrada, Y.O., Genova, R.C., *et al.*, Eds.; Cambridge University Press: Cambridge, UK; New York, NY, USA, 2014; pp. 361–409.
49. Wong, P. Impacts and recovery from a large tsunami: Coasts of Aceh. *Pol. J. Environ. Stud.* **2009**, *18*, 5–16.
50. IPCC. Contribution of Working Groups I, II and III to the Fourth Assessment Report of the Intergovernmental panel on climate change. In *Climate change 2007: Synthesis Report*; IPCC: Genewa, Switzerland, 2007.
51. Defra. Adapting to climate change UK climate projections. *UK Clim. Proj.* **2009**, *52*, 1–42.
52. Lowe, J.; Howard, T.; Pardaens, A.; Tinker, J.; Holt, J.; Wakelin, S.; Milne, G.; Leake, J.; Wolf, J.; Horsburgh, K. *UK Climate Projections Science Report: Marine and Coastal Projections*; Met Office Hadley Center: Exeter, UK, 2009.
53. NOAA Coastal Service Center. Detailed Methodology for Mapping Sea Level Rise Inundation. 2002. Available online: http://coast.noaa.gov/slr/assets/pdfs/Inundation_Methods.pdf (accessed on 10 January 2014).
54. Avtar, R.; Yunus, A.P.; Kraines, S.; Yamamuro, M. Evaluation of DEM generation based on interferometric SAR using TanDEM-X data in Tokyo. *Phys. Chem. Earth Parts A/B/C* **2015**, *83–84*, 166–177. [CrossRef]
55. Horton, B.P.; Rahmstorf, S.; Engelhart, S.E.; Kemp, A.C. Expert assessment of sea-level rise by AD 2100 and AD 2300. *Quat. Sci. Rev.* **2014**, *84*, 1–6. [CrossRef]
56. Kopp, R.E.; Horton, R.M.; Little, C.M.; Mitrovica, J.X.; Oppenheimer, M.; Rasmussen, D.; Strauss, B.H.; Tebaldi, C. Probabilistic 21st and 22nd century sea-level projections at a global network of tide-gauge sites. *Earth's Future* **2014**, *2*, 383–406. [CrossRef]
57. FEMA. *Standards for LiDAR and Other High Quality Digital Topography. Procedure Memorandum No. 61*; US Department of Homeland Security: Washington, DC, USA, 2010.
58. Farr, T.G.; Rosen, P.A.; Caro, E.; Crippen, R.; Duren, R.; Hensley, S.; Kobrick, M.; Paller, M.; Rodriguez, E.; Roth, L. The shuttle radar topography mission. *Rev. Geophys.* **2007**, *45*, 1–42. [CrossRef]
59. Cooper, H.M.; Fletcher, C.H.; Chen, Q.; Barbee, M.M. Sea-Level rise vulnerability mapping for adaptation decisions using LiDAR DEMs. *Prog. Phys. Geogr.* **2013**, *37*, 745–766. [CrossRef]
60. Zhang, K. Analysis of Non-Linear inundation from sea-level rise using LiDAR data: A case study for south Florida. *Clim. Chang.* **2011**, *106*, 537–565. [CrossRef]
61. Dasgupta, S.; Laplante, B.; Meisner, C.; Wheeler, D.; Yan, J. The impact of sea level rise on developing countries: A comparative analysis. *World Bank Policy Res. Work. Pap.* **2007**, *4136*, 1–51.
62. ESRI. Resample (Data Management). Available online: http://help.arcgis.com/EN/arcgisdesktop/10.0/help/index.html#//001700000009t000000 (accessed on 15 September 2015).
63. Griffin, J.; Latief, H.; Kongko, W.; Harig, S.; Horspool, N.; Hanung, R.; Rojali, A.; Maher, N.; Fountain, L.; Fuchs, A.; *et al.* An evaluation of onshore digital elevation models for tsunami inundation modelling in Indonesia. In Proceedings of the 37th HAGI Annual Convention & Exhibition, Pelembang, Indonesia, 10 September 2012; pp. 1–16.
64. Hayakawa, Y.S.; Oguchi, T.; Lin, Z. Comparison of new and existing global digital elevation models: ASTER G-DEM and SRTM-3. *Geophys. Res. Lett.* **2008**, *35*. [CrossRef]
65. Wang, W.; Yang, X.; Yao, T. Evaluation of ASTER GDEM and SRTM and their suitability in hydraulic modelling of a glacial lake outburst flood in Southeast Tibet. *Hydrol. Process.* **2012**, *26*, 213–225. [CrossRef]
66. Di Baldassarre, G.; Uhlenbrook, S. Is the current flood of data enough? A Treatise on research needs for the improvement of flood modelling. *Hydrol. Process.* **2012**, *26*, 153–158. [CrossRef]

67. Gallegos, H.A.; Schubert, J.E.; Sanders, B.F. Two-Dimensional, high-resolution modelling of urban dam-break flooding: A case study of baldwin hills, California. *Adv. Water Resour.* **2009**, *32*, 1323–1335. [CrossRef]
68. Schumann, G.; Di Baldassarre, G.; Bates, P.D. The Utility of spaceborne radar to render flood inundation maps based on multialgorithm ensembles. *IEEE Trans. Geosci. Remote Sens.* **2009**, *47*, 2801–2807. [CrossRef]